Biosensors and Bioelectronics 144 (2019) 111639

Contents lists available at ScienceDirect

Biosensors and Bioelectronics

journal homepage: www.elsevier.com/locate/bios

Plasmonic droplet screen for single-cell secretion analysis

Shih-Chung Wei[a], Myat Noe Hsu[b], Chia-Hung Chen[a,b,*]

[a] Institute for Health Innovation & Technology, National University of Singapore, 117599, Singapore
[b] Department of Biomedical Engineering, National University of Singapore, 117574, Singapore

ARTICLE INFO

Keywords:
Single cell analysis
Surface plasmon resonance
Multiplex detection
Immunoassay
Platform engineering

ABSTRACT

Single-cell secretion analysis technologies are needed to elucidate the heterogeneity of cellular functionalities. Although ligand binding assays in microwells provide a promising approach for measuring single-cell secretions, their throughput is limited. Recently, droplet assays have been developed for high-throughput single-cell screening. However, because washing steps are difficult to perform with droplets, there are still challenges in measuring secretions using droplet assays. In this study, a plasmonic droplet screen approach is developed for one-step washing-free multiplex detection of single-cell secretions. Individual cells are encapsulated with antibody-conjugated gold nanorods (AuNRs) in droplets to evaluate their secretion levels. The shift in the plasmon resonance peak reflects the amount of secreted protein without needing additional indicator and washing steps. The plasmonic signals from a continuous flow of single-cell droplets are collected by dark-field spectroscopy (~100–150 cells min^{-1}). This platform is tested by screening interleukin-8 (IL-8) and vascular endothelial growth factor (VEGF) secreted from suspended leukemia cells and adherent breast cancer cells. Overall, this novel strategy shows the potential and flexibility of high-efficiency multiplex single-cell secretion analysis.

1. Introduction

Analytical tools for cell genotyping and phenotyping have promoted the development of new diagnostic strategies and the modern bioindustry (Bousman and Dunlop, 2018). Recently, alternative single-cell approaches have improved the screening processes for genomic (Marcy et al., 2007) and proteomic profiling (Heath et al., 2015). For example, cells with mutations and genome editing could be screened and identified by a single-cell analysis platform such as Fluidigm (Cheow et al., 2016). However, without an effective tool for analyzing secretions from individual cells, there are still challenges in obtaining a complete understanding of cell functionality and activity (Obenauf et al., 2015; Xue et al., 2008).

At present, single-cell proteomics are mainly investigated by two platforms: flow cytometry and multiwell technologies (Lu et al., 2017). Commercial flow cytometers with a throughput of 1000–10,000 cells sec^{-1} have been broadly used to identify single cell surface biomarkers and intracellular proteins (Bendall et al., 2011; Spitzer and Nolan, 2016). In addition, deformability cytometry was recently developed to determine the mechanophenotype of individual cells (Tse et al., 2013). However, although high-throughput screening could be performed by flow cytometry, this technique is not flexible enough for measuring cellular secretions (Fiehn, 2002).

A multiwell ligand binding approach provides a relatively flexible platform for a range of single-cell secretion analysis. Recently, multiplex detection for single-cell secretions were achieved by antibody barcode arrays (Lu et al., 2015) or microengraving (Bradshaw et al., 2008). Tay S. et al. demonstrated multiplexed cytokine reaction kinetics measurement via a cell trapping microchamber (Junkin et al., 2016). However, despite the flexibility of the multiwell binding assay in target selection, the throughput of multiwell approaches is limited by the number of wells (~100–1000 per experimental run). Hence, screening a large number of cells remains a challenge.

Recently, droplet-based microfluidics have emerged as a high-throughput single-cell detection technique (Mazutis et al., 2013). Cells are dispersed into oil phase to form isolated water-in-oil (w/o) droplets for high-throughput single-cell screening (~1000 droplets/second). In 2007, Huebner A. et al. demonstrated single-cell protein expression measurement by using droplet-based microfluidics (Huebner et al., 2007). In 2010, Weitz D. A. et al. pioneered the utilization of an high-throughput single-cell droplet screening method for directed enzyme evolution (Agresti et al., 2010). After that, various single-cell droplet methods were developed for diagnosis, metabolic engineering, and synthetic biology. For example, protease activity analysis for single circulating tumor cell (Dhar et al., 2018), single bacteria selection based on metabolite enzymatic assay (Wang et al., 2014), and

* Corresponding author. Department of Biomedical Engineering, City University of Hong Kong, 83 Tat Chee Avenue, Kowloon Tong, Hong Kong.
E-mail address: chiachen@cityu.edu.hk (C.-H. Chen).

https://doi.org/10.1016/j.bios.2019.111639
Received 10 May 2019; Received in revised form 11 August 2019; Accepted 26 August 2019
Available online 31 August 2019
0956-5663/

fluorescence resonance energy transfer (FRET) substrates for determining metalloproteinase activity (Ng et al., 2019). However, these enzymatic assays only sense analytes with enzymatic activity.

Droplet-based immunoassay was developed to measure secreted proteins and metabolites. For example, microbeads sensor and human serum were encapsulated within droplets for C-reactive protein immunoassay with detection limitation of 0.01 μg ml^{-1} (Tang and Shum, 2016). Single T-cell secretion of IL-10 was measured via droplet based approach with detection limitation of 10 pg ml^{-1} (Konry et al., 2011). The agarose particles containing single Jurkat T-cell and functionalized capture beads were washed for subsequent cytokine immunoassay (Chokkalingam et al., 2013). The alginate particles containing antibody, reporters and cells were encapsulated within the droplets. After that, the particles were washed for anti-TNF-alpha antibody screening (Akbari and Pirbodaghi, 2014). Functional hydrogel particles such as poly (N-isopropylacrylamide) particles were used to concentrated fluorophore conjugated antibodies within the particles to enhance detection sensitivities (500 pg ml^{-1}) (Hsu et al., 2018). However, these immunoassay approaches required breaking the droplets to perform washing process of hydrogel particles, which caused the limitation for cell sorting after screening. Recently, analyte-responsive RNA aptamers sensors and magnetic bead sensors were investigated to perform washing-free droplet-based immunoassay (Eyer et al., 2017). However, due to the high background of blank droplets, the detection limit of this approach was ~150 ng/ml (Eyer et al., 2017). To address this issue, a fluorescence normalization algorithm was implemented, improving the detection limit to 50 ng/ml (Shembekar et al., 2018).

In this study, a one-step and washing-free plasmonic droplet sensor with high sensitivity (6–7 ng/ml)was developed. This sensor provides a label-free, high-throughput, and multiplexable platform for monitoring single-cell secretions without breaking the droplet (Fig. 1a). Because of low toxicity to the cells and wide spectra distribution for multiplexed assay, gold nanorods (AuNR) were used as the plasmonic sensors in this study. The binding of analytes affects the aggregation of AuNRs and causes the differences in localized surface plasmon resonance (LSPR) spectrum shift (Fig. 1b). This approach does not require additional indicators and washing steps. Plasmonic droplets in a continuous flow were detected by a dark-field spectroscope (600–1800 droplets min^{-1}; 100–150 cells min^{-1}) for high-throughput screening. We demonstrated the utility of this sensor by determining the secretion level of interleukin-8 (IL-8) and vascular endothelial growth factor (VEGF) from both suspended and adherent cancer cells. This technology builds on prior successes in Au cluster sensor in droplets assay (Shen et al., 2018). To the best of our knowledge, this work is the first multiplexed plasmonic droplet for high-throughput single-cell cytokine secretion analysis.

2. Experimental section

2.1. Cell culture and staining

Cells of a human breast cancer cell line (MDA-MB-231) and a human promyelocytic leukemia cell line (HL-60) were purchased from American Type Culture Collection (VA, USA). MDA-MB-231 cells were cultured in Dulbecco's modified Eagle medium (DMEM) from Gibco with 10% inactivated fetal bovine serum (Gibco, MA, USA) and 50 μg ml^{-1} gentamicin (Gibco, MA, USA). Suspended HL-60 cells were cultured in Iscove's modified Dulbecco's medium (IMDM) from Gibco with 20% inactivated fetal bovine serum (Gibco, MA, USA) and 50 μg ml^{-1} gentamicin (Gibco, MA, USA). All cells were incubated at 37 °C in an incubator with 5% CO2 and were grown to > 80% confluency for single-cell experiments. Cells were washed twice and concentrated to 1 million cells ml^{-1} in medium for lipid staining. For staining, 10 μl of the lipophilic carbocyanine DiR (Thermo Fisher, MA, USA) dissolved in ethanol was added into a 1 ml cell suspension and incubated at 37 °C for 20 min. Two additional washes were performed, and the cells were resuspended in reaction buffer as mentioned in the plasmonic sensor section for plasmonic sensing. Recombinant human TNF-α protein (CF210-TA/CF) from R&D Systems (MN, USA) was mixed into the cell suspension to stimulate cellular secretion. The cell suspension was then passed through a cell strainer with a pore size of 40 μm. The final cell density for droplet encapsulation was approximately 5–10 million cells ml^{-1}.

2.2. Conventional Enzyme-Linked immunosorbent assay (ELISA)

The Human IL-8/CXCL8 Quantikine ELISA Kit (D8000C) purchased from R&D Systems (MN, USA) was used for the Enzyme-Linked immunosorbent assay (ELISA) experiment. For sample preparation, cells were cultured in a 96-well microplate for one day. The initial cell density was three thousand cells per well. After one day, the culture medium was replaced with fresh culture medium, medium with TNF-α, nanorod solution, or nanorod solution with TNF-α. The cells were incubated for another 24 h for secretion. The supernatant was then harvested for the secretory protein level test.

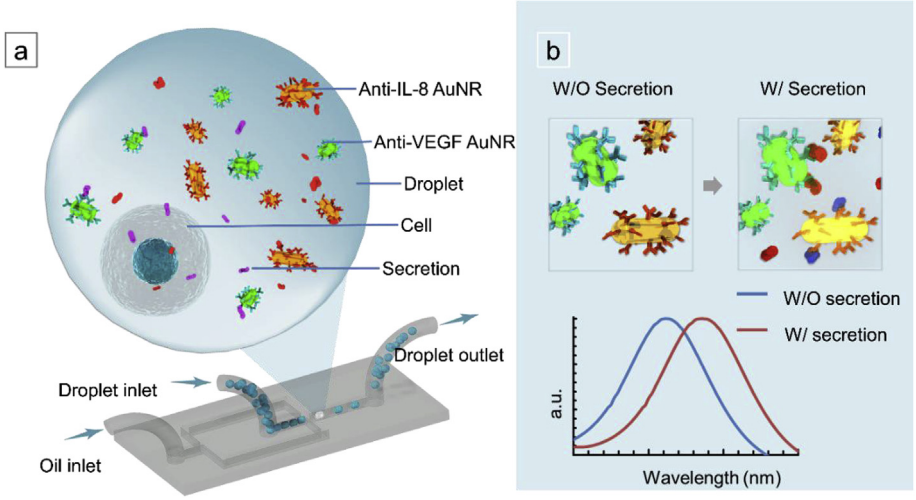

Fig. 1. (a) Schematic of the plasmonic droplet-screening immunoassay for single-cell secretion screening. (b) The scattering spectrum of the nanorods was shifted after assaying in the buffer.

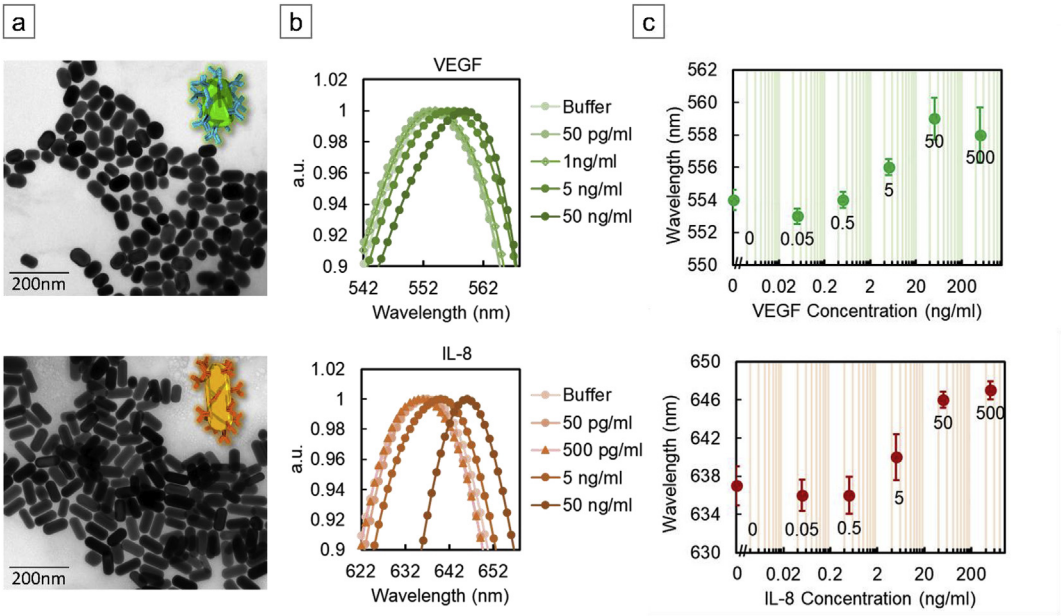

Fig. 2. (a) Transmission electron microscopy (TEM) image of VEGF antibody-conjugated nanorods (aspect ratio: 1.5) and IL-8 antibody-conjugated nanorods (aspect ratio: 2.4). (b) The absorption spectrum of VEGF and IL-8 antibody-conjugated nanorods was measured with a UV–visible spectrometer after adding the target at a series of concentrations. The resonant peaks are plotted in (c).

2.3. Gold nanorod (AuNR) functionalization

Anti-VEGF-conjugated AuNRs with a 1.5 aspect ratio and 50 O.D. were used. Anti-IL-8-conjugated AuNRs with a 2.4 aspect ratio were customized by Creative Diagnostics (NY, USA). Human VEGF165 antibody (AF-293-NA) and human IL-8/CXCL8 antibody (MAB208) purchased from R&D Systems (MN, USA) were conjugated to the AuNRs through a COOH-terminated PEG thiol linker. The linker was attached to the AuNR surface through spontaneously formed Au–S bonds. The COOH group of the linker was then activated by 10 mg ml^{-1} 1-ethyl-3-(3-dimethylaminopropyl) carbodiimide hydrochloride (EDC) and N-hydroxysulfosuccinimide sodium salt (NHS) for 30 min. The surface activated AuNRs were mixed with antibodies to form peptide bonds. Anti-mouse IgG-conjugated gold nanorods were purchased from Nanopartz (CO, USA) for system verification in the supplemental experiments.

2.4. Plasmonic sensor

A reaction buffer was prepared for all dilutions in this study. The composition of the reaction buffer was 70 mmol L^{-1} sodium chloride (NaCl), 1.5 mmol L^{-1} potassium chloride (KCl), 5 mmol L^{-1} sodium phosphate dibasic (Na_2HPO_4), and 11 mmol L^{-1} potassium phosphate monobasic (KH_2PO_4). All the chemicals used for buffer preparation were from Sigma-Aldrich (MO, USA). The pH of the buffer was adjusted to 7.4 before use. Recombinant human VEGF 165 protein (293-VE), recombinant human IL-8/CXCL8 protein (208-IL), and normal human IgG control (1-001-A) were purchased from R&D Systems (MN, USA) as control ligands. These control ligands were diluted to different concentrations with reaction buffer for assay characterization. The antibody-conjugated AuNR sensors were diluted 100 times in reaction buffer for the bulk experiment. The diluted AuNR solution was incubated with control ligands in a 96-well microplate for 24 h, and the absorption spectrum was measured using a UV–visible spectrometer. The antibody-conjugated AuNR sensors were diluted 24 times in reaction buffer for droplet encapsulation. For characterization, AuNR sensors and control ligands were co-encapsulated in oil and incubated for 2 h. For single-cell secretion screening, AuNR sensors were combined with a cell suspension and incubated for 24 h before observation. For multiplex detection, AuNRs for VEGF and IL-8 were mixed together at a ratio of 1.5:1.

2.5. Droplet encapsulation

Droplet encapsulation was conduct with PDMS microfluidics. The procedure of PDMS chip fabrication and the characterization of the wafer mold are in Fig. S1. The droplet-generating microfluidic device made of PDMS had three inlets for the 1) AuNR solution; 2) sensing target, which was the control ligand solution or the cell suspension; and 3) oil phase (Fig. S1b). The PDMS microfluidic chip was heated to 120 °C for 10 min and cooled to room temperature before use. The AuNRs and sensing targets were loaded into the droplet-generating microfluidic device via syringe pumps. These two solutions were mixed in a pinched flow channel for encapsulation. The oil phase was prepared by adding 3% Pico-Surf 1 (Blacktrace Holdings Ltd., UK) to NOVEC 7500 (3M, MN, USA) engineered fluid. The flow rate of both aqueous phases was 2 µl min^{-1}, and the flow rate of the oil phase was 5 µl min-1. For single-cell encapsulation, cell density was 5–10 million cells ml^{-1}. Cell solution was gently vortexed with rotating magnet in the syringe.

2.6. Scattering spectrum acquisition

Droplet screening was performed on an inverted dark-field spectroscope (Fig. S2). Laser-driven xenon light with a broadband spectrum (EQ-99X LDLS, Energetiq Technology, MA, USA) was used for illumination. The scattered light from AuNRs was collected by an inverted dark-field microscope (Eclipse Ti–U, Nikon, JP). The collected light was passed through a slit to eliminate out-of-focus scattering. The scattered light was dispersed into a spectrum by a Shamrock 303i spectrometer (ANDOR Technology Ltd, NIR). The spectrum was then recorded using a Newton 940 spectroscopic CCD camera (Andor Technology Ltd, NIR). For static screening, droplets were loaded into an observation chamber made of PDMS. We scanned through the highly packed droplets in the chamber with a 5 µm step size for collecting the scattering spectrum with a stage scanner (SCAN IM Plus 130 × 85 XY Stage, MÄRZHÄUSER WETZLAR GMBH & CO., DE). For high-throughput screening, the droplets were loaded into a PDMS continuous flow channel, and spacing oil

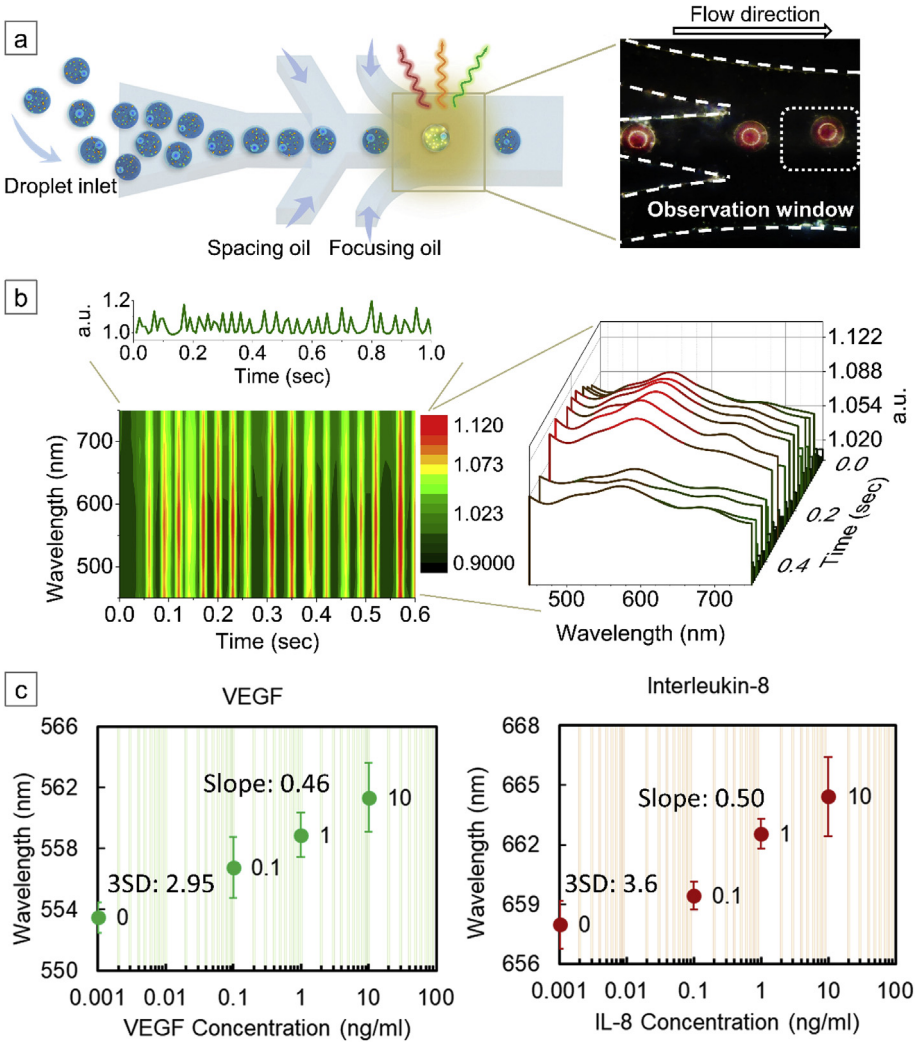

Fig. 3. (a) High-throughput screening with the plasmonic droplet sensor was conducted with continuous-flow microfluidics and dark-field spectroscopy. A focusing flow from both sides could prevent scattered light coming from the edge of the microfluidic channel. (b) A time series spectrum was acquired with the spectrometer in dynamic mode. The highest scanning rate attained was 30–50 droplets sec^{-1} with a 0.01 s acquisition time (100 frame sec^{-1}). (c) Functional tests of IL-8 and VEGF plasmonic droplet sensors. The result was calculated from approximately 3000 droplets.

was used to separate individual droplets (Fig. S1c). The droplets were focused in a central stream by focusing oil. The flow rate of the droplets was 0.1 μL min^{-1}, and the flow rate of the oil phase was 1 μL min^{-1}. To ensure that the signal arose from single droplets, the light entrance of the spectrometer was controlled to be smaller than the dimension of the droplet images at the slit. The scattered light was then dispersed into a spectrum by an optical grating inside the spectrometer. Finally, the spectra from individual droplets were recorded by a spectroscopic CCD detector. The irradiation with wavelength from 450.02 nm to 998.63 nm was recorded by a 2048*512 sensing array. The accuracy for peak measurements was one pixel, which was 0.27 nm (Martinez-de Dios and Ollero, 2004).

3. Results and discussion

3.1. Plasmonic droplet sensor

Plasmonic droplet sensors in this work are based on measuring the LSPR spectra of functionalized AuNRs within the droplets. LSPR is a collective oscillation of electrons, which resonate at a specific wavelength, in nanoparticles (Cao et al., 2014). The resonant wavelength is determined by the material, shape and near-field refractive index change of the nanoparticles. Once AuNR aggregate with each other or analytes bind to the AuNR, the resonance changes. The light scattering and absorption of nanoparticles at specific wavelengths are broadly used to investigate the resonance wavelength. In this work, we characterized the synthesized AuNRs by light absorption, and monitored the AuNR status in droplets by light scattering instead. For cell screening, suspended cells were mixed with the AuNR sensor in the microfluidics to form water-in-oil (w/o) emulsions. After 24 h of incubation, we screened these plasmonic droplets in a continuous flow by the dark-field spectroscope. The throughput of droplet screening is 600 droplet min^{-1}. Shift of the plasmonic scattering peak represented the secretion level of the cells.

3.2. Plasmonic sensor (AuNR) characterization

The dimension of AuNRs were characterized by transmission electron microscopy (TEM) (Fig. 2a). The aspect ratios were 1.5 ± 0.23 and 2.4 ± 0.36 for the VEGF AuNR and the IL-8 AuNR, respectively (Figs. S3a and b). The conjugation of VEGF antibody and IL-8 antibody on AuNRs were verified by the negative value of zeta potential (Fig. S3c). Calibration curves were generated to characterize the functionality of AuNR sensors. We spiked analytes at different concentrations into the AuNR solutions. The mixtures were incubated for 24 h. The shifts of AuNR absorption spectra in Fig. 2b indicates different

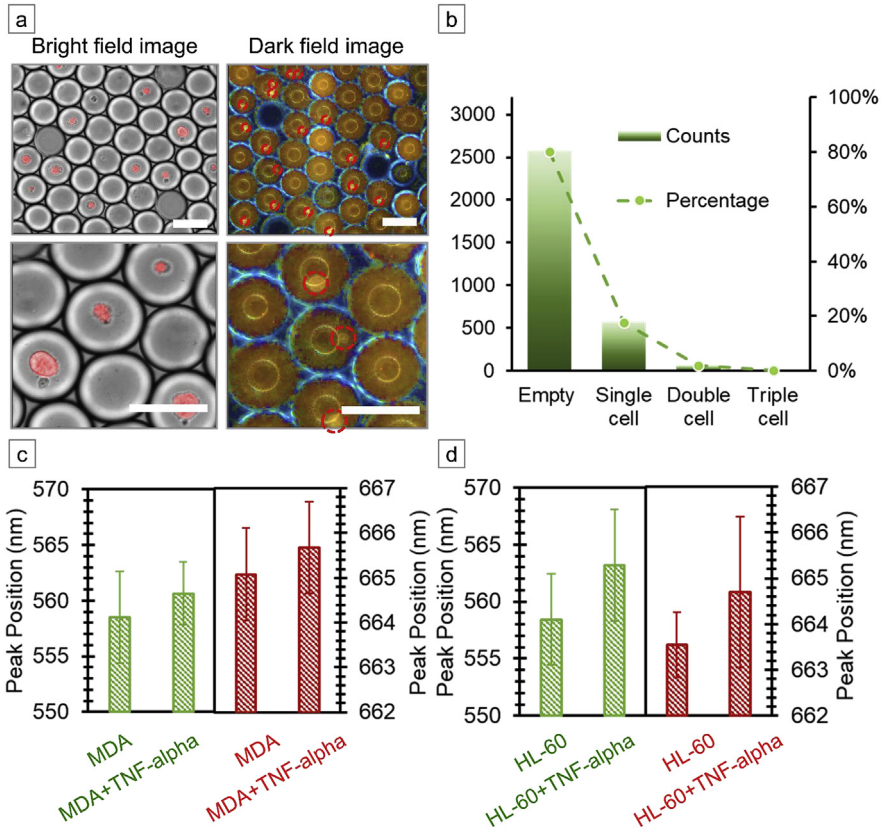

	VEGF		IL8		VEGF		IL8	
	MDA	MDA+TNF	MDA	MDA+TNF	HL60	HL60+TNF	HL60	HL60+TNF
Mean	558.489	560.652	558.443	563.17	665.081	665.68	663.554	664.707
SD	4.125	2.797	4.008	4.917	1.035	1.015	0.714	1.64836

Fig. 4. (a) Bright-field image and dark-field image of a cell encapsulated in plasmonic droplets. (b) The single-cell encapsulation rate reached 17–20%. The plasmonic droplet sensor could identify different VEGF and IL-8 secretion profiles after (c) MDA-MB-231 and (d) HL-60 cells were treated with TNF-α (scale bar: 50 μm). Unpaired two sample t-tests were performed to verify the means of TNF-alpha treated group and non-treated group have significant difference ($p < 0.05$).

aggregation status and number of bonded ligands The statistical analysis of peak positions is plotted in Fig. 2c. The sensitivity is 0.44 nm (ng $ml^{-1})^{-1}$ for VEGF AuNRs and 0.88 nm (ng $ml^{-1})^{-1}$ for IL-8 AuNRs. Notably, the ion concentration of the salt affected the peak shift (Fig. S4a). The ionic strength of the salt in a solution decreased surface charge repulsion to cause some aggregations of the AuNRs. This process required ~8 h to be stable in our experiment for the measurements (Fig. S4b). The stability of functionalized AuNRs in 24 h incubation was characterized to correspond to the incubation time period of the measurements (Fig. S4c).

3.3. Plasmonic droplet sensing

To ensure the functionality of the plasmonic sensor in droplets, target biomolecules at different concentrations were mixed with AuNRs in droplets. After incubation, the droplets were injected into a PDMS observation chamber. Approximately 50–100 droplets were observed for each reaction condition by line scanning (Fig. S5a). Because of the limited optical path inside a droplet (~50 μm diameter), a scattering spectrum was acquired instead of an absorption spectrum to monitor the plasmon resonance. The scattering peak was then analyzed to quantify the binding of target biomolecules to the AuNR surface. The averaged absorption spectra used for characterization are plotted in Fig. S5b. As expected, a shift was observed corresponding to the target concentration. This shift was also observed in the heat map of the scattering spectra from individual droplets in the chamber (Fig. S5c).

Characterization of the plasmonic droplet sensor in a continuous flow was then performed. After 24 h of incubation, the droplets were loaded into a microfluidic channel for continuous flow screening by dark-field spectroscopy (Fig. 3a). The screening protocol was described in Sec. 2.6. To acquire enough scattering light under continuous flow, the opening of the slit was 500 μm (Fig. S6a). The signal collection capability at different acquisition time was also investigated (Fig. S6b). Peak analysis indicated that the peak positions were not affected by the sampling rate (Fig. S6c). The spectra of plasmonic droplets passing through the observation window were recorded in real time and are plotted in Fig. 3b. Individual yellow/red lines in the heat map represent a single droplet. The droplet scanning rate was calculated from the signal intensity peak number over time. The highest scanning rate attained was 1800 droplets min^{-1} for plasmonic droplet characterization.

Calibration curve were generated for VEGF plasmonic droplet sensor and IL-8 plasmonic droplet sensor in Fig. 3c. AuNRs and analytes at different concentration were mixed in microfluidics to form droplets. After overnight incubation, the droplets were screened followed the protocol described in Sec. 2.6. The peaks of the scattering spectra were measured to correspond to the spiked analyte concentrations. The sensitivity of droplet plasmonic assay to measure VEGF was 0.46 nm/(ng/ml), while sensitivity to measure IL-8 was 0.50 nm/(ng/ml). The limit of detections to measure VEGF was 6.39 ng/ml, and the limit of detection to measure IL-8 was 7.2 ng/ml.

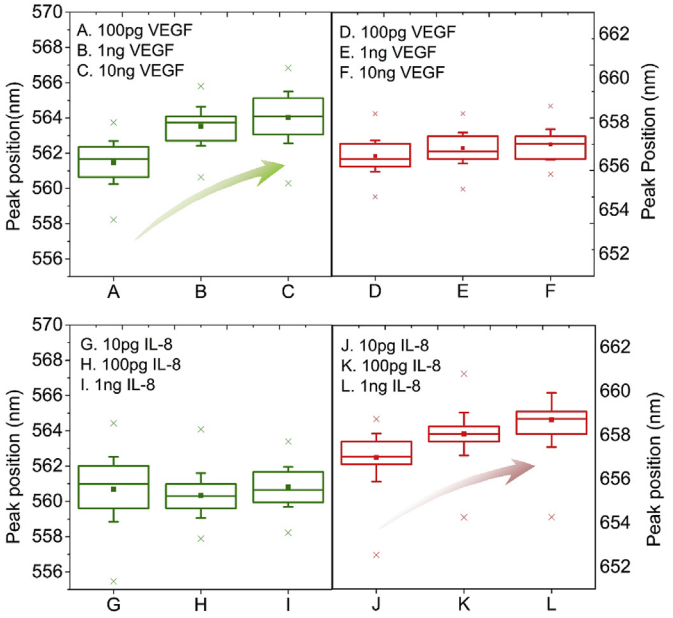

Fig. 5. Specificity was tested for multiplex detection. For A-F, only VEGF was added. The peak position of anti-VEGF AuNRs (A–C) was redshifted with increasing VEGF concentration, while anti-IL-8 AuNRs (D–F) showed a consistent peak position. For G-L, only IL-8 was spiked into the reaction. The peak position of anti-IL-8 AuNRs (J–L) increased with the IL-8 concentration, while the peak position of anti-VEGF AuNR (G–I) remained consistent.

3.4. Single-cell secretion screening

Cellular secretions (VEGF and IL-8) from two different cancer cells (the MDA-MB-213 breast cancer cell line and the HL-60 leukemia cell line) were measured via the plasmonic droplet screen immunoassay. These cells were prepared as described in Sec. 2.1.

The overlaid bright-field and fluorescence image of droplets with cells is shown in the left part of Fig. 4a. The dark-field image in the right part of Fig. 4a was recorded to show the AuNR sensor in the droplets. The single-cell encapsulation rate reached 17%–20% through optimization of the flow rate and cell concentration (Fig. 4b). These droplets with cells were incubated at 37 °C for 24 h before observation. Then, continuous flow screening was performed with a throughput of ~600 droplets min^{-1} (~100–150 cells). The stability of the droplets is shown in Fig. S7. The cell viability of HL-60 and MDA-MB-231 in droplet is shown in Fig. S8.

The MDA-MB-231 secretion results are shown in Fig. 4c. With TNF-α stimulation, a slight increase in the average level of VEGF was observed. These results agree with the results of ELISA (Fig. S9). The levels of IL-8 also increased (Freund et al., 2004; He et al., 2003). The VEGF and IL-8 secretion levels of HL-60 cells are shown in Fig. 4d. For cells with TNF-α stimulation, increases in both VEGF and IL-8 secretion levels were observed (He et al., 2003). According to the results, the VEGF secretion level was similar among MDA-MB-231 and HL-60 cells before stimulation, while MDA-MB-231 cells secreted more IL-8. However, after stimulation, TNF-α increased IL-8 secretion in HL-60 cells largely than in MDA-MB-231 cells. The IL-8 secretion of HL-60 cells with incubation time is shown in Fig. S10. The result indicates that the peak of IL-8 in HL-60 cells shifted from 656 nm to 663.5 nm after 24 h of stimulation. The statistical analytical method used to evaluate single cell's secretions is included in Fig. S11.

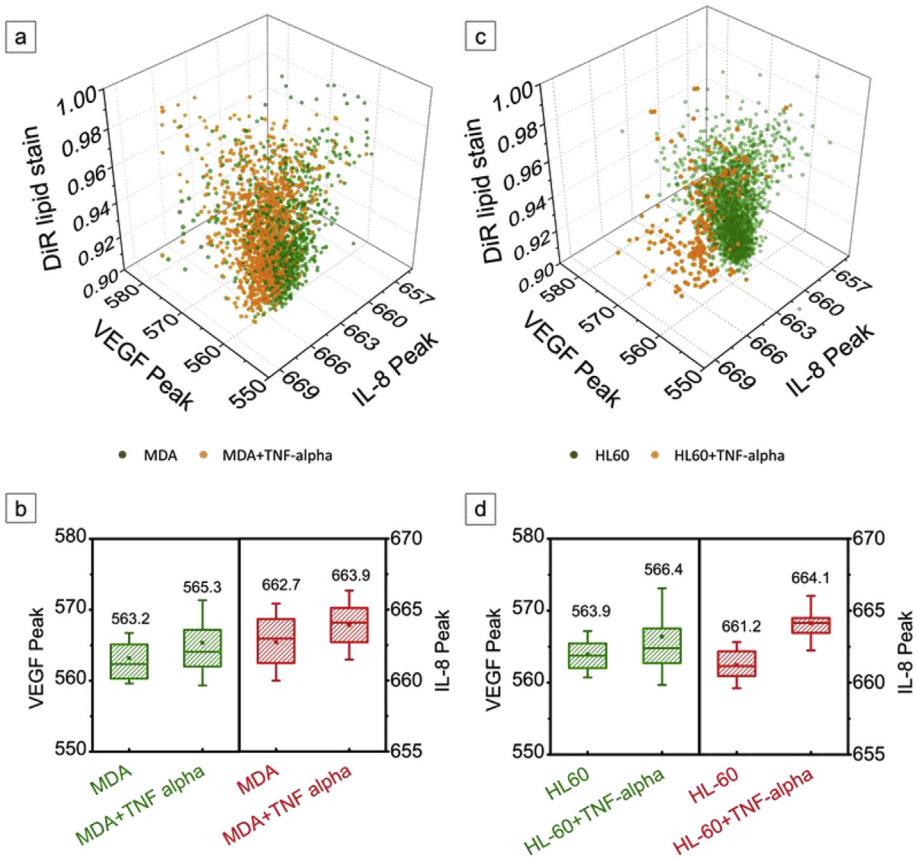

Fig. 6. (a) Two groups of MDA-MB-231 cells could be identified as stimulated and unstimulated cells. (b) The box plot shows the secretion level increase after stimulation. (c) A similar grouping could be found in the HL-60 results. (d) The box plot shows a similar trend of increased secretion by HL-60 cells.

3.5. Multiplex detection for single-cell secretion screening

AuNRs with different aspect ratios were mixed to achieve multiplex plasmonic droplet assay (Tang and Casas, 2014; Yu and Irudayaraj, 2007). Two types of AuNRs with scattering peaks at 556 nm and 658 nm were used. To clearly identify the peaks, the balance of scattering intensity was optimized by adjusting the concentrations of the AuNRs (Fig. S12). The positions of the two peaks were closer to each other after mixing. The peak of the anti-VEGF AuNRs became ~561 nm, and the peak of the AuNRs conjugated with anti-IL-8 moved slightly to ~657 nm. In addition, mixed solutions with different concentrations of VEGF and IL-8 were evaluated for specificity to ensure that spectral crosstalk did not cause false results (Fig. 5).

The AuNR mixture was encapsulated with individual cells in the droplets. These plasmonic droplets with cells were incubated at 37 °C for 24 h before observation. Based on the multiplex detection results, VEGF secretion, IL-8 secretion and DiR lipid staining were measured simultaneously to form a three-dimensional plot. For MDA-MB-231 cells (Fig. 6a), as expected, two distinct clusters were observed, indicating the presence of TNF-α-treated and nontreated cells. Statistical analysis between different groups was performed to reveal the trends for shifts in the scattering peak (Fig. 6b). VEGF and IL-8 secreted by MDA-MB-231 cells slightly increased after stimulation. Similar to the results for MDA-MB-231 cells, HL-60 cells exhibited distinct clusters (Fig. 6c). Statistical analysis of HL-60 cells also indicated increased VEGF and IL-8 secretion after TNF-α stimulation (Fig. 6d). The multiplex detection results are consistent with the singleplex detection results.

4. Discussion

The plasmonic droplet immunoassay was developed by integrating localized surface plasmonic sensors and continuous flow droplet picoreactors. The plasmonic sensor has minimized the complexity of performing an immunoassay in droplets to achieve the goal of rapidly identifying single-cell secretory phenotypes. The sensitivity of VEGF assay is 0.46 nm/(ng/ml) and sensitivity of IL-8 assay is 0.50 nm/(ng/ml). The limit of detections were 6.39 ng/ml and 7.2 ng/ml for VEGF assay and IL-8 assay, respectively. The detection sensitivity of plasmonic droplet assay is comparable to the sensitivity of current fluorescence based drop-screen approaches (Konry et al., 2011; Hsu et al., 2018). However, with the advantage of washing-free detections via plasmonic assay, after plasmonic drop screening, the droplets with cells could be sorted and collected for the applications in bio-fabrication and synthetic biology.

The resonant frequency change caused by AuNRs aggregation is sensitive to the ligand binding on AuNR surface. The variation of plasmonic peak position measurement might be due to technical noise or the aspect ratio variation of AuNRs (Tadepalli et al., 2015). Reduced variation is expected by upgrading the transducer (such as a liquid nitrogen-cooled camera), using a high-intensity light source (such as a high-power mercury-xenon light) and minimized the size variation in the AuNRs.

The throughput of cell screening was limited by the required integration time for recording cell tracker fluorescence (~600 droplets min^{-1}). This could be improved by using a brighter cell tracker or stronger excitation irradiation to reduce the spectrum acquisition time. Moreover, the sensitivity could be improved by enhancing the refractive index change when target molecules binding (Teste and Descroix, 2012). It is worth noting that to perform plasmonic drop-screen it is essential to suspend the cells in a solution. To detach the cells from the substrates, the cell survival rates would be effected. Especially for no-metastatic adherent cells, dissociation of the cells to a solution would initiate programmed cell death (anoikis). Moreover, due to limited nutrition within the droplets, long-term cell incubation (over 3 days) could not be processed properly in the droplets.

5. Conclusion

In this study, we described a droplet-based wash-free sensor that enables one-step and effective single-cell multiplex secretion analysis. The sensitivity of plasmonic droplet assay is around 0.5 nm/(ng/ml). The limit of detections were 5.9 ng/ml and 7.2 ng/ml for VEGF and IL-8, respectively. The VEGF and IL-8 secretion levels of MDA-MB-231 breast cancer cells and HL-60 leukemia cells were measured with a throughput of ~600 droplets min^{-1} as a demonstration of this technology. With TNF-α stimulation, changes in secretion profiles were observed. By loading AuNRs with different aspect ratios, a multiplex plasmonic droplet screen immunoassay was achieved. Although further optimization could be conducted, this platform still represents a promising tool for single-cell secretion analysis, increasing the applicability of single-cell functional analysis. More applications of plasmonic droplet screen platforms in engineering biology, disease diagnosis, and treatment support are expected after their improvement in the future. For instance, analysis of cancer metastasis related secretory proteins, immune cells response, and target screening in enzymatic engineering and synthetic biology.

CRediT authorship contribution statement

Shih-Chung Wei: Formal analysis, Writing - original draft. **Myat Noe Hsu:** Formal analysis, Writing - original draft. **Chia-Hung Chen:** Writing - original draft, Supervision.

Declaration of competing interest

The authors declare that they have no conflict of interest that could have appeared to influence the work reported in this paper.

Acknowledgements

The authors gratefully acknowledge the funding provided by NMRC OFIRG (R-397-000-289-213), NRF CRP (R-397-000-276-281), NRF EIRP (R-397-000-252-592), NRF BDTA (R-397-000-221-592), and MOE Tier-2 (R-397-000-271-112, R-279-000-501-112, and R-397-000-253-112).

Appendix A. Supplementary data

Supplementary data to this article can be found online at https://doi.org/10.1016/j.bios.2019.111639.

References

Agresti, J.J., Antipov, E., Abate, A.R., Ahn, K., Rowat, A.C., Baret, J.-C., Marquez, M., Klibanov, A.M., Griffiths, A.D., Weitz, D.A., 2010. Proc. Natl. Acad. Sci. U.S.A. 107 (9), 4004–4009.
Akbari, S., Pirbodaghi, T., 2014. Lab Chip 14 (17), 3275–3280.
Bendall, S.C., Simonds, E.F., Qiu, P., Amir, E.-a.D., Krutzik, P.O., Finck, R., Bruggner, R.V., Melamed, R., Trejo, A., Ornatsky, O.I., Balderas, R.S., Plevritis, S.K., Sachs, K., Pe'er, D., Tanner, S.D., Nolan, G.P., 2011. Science (New York, N.Y.) 332 (6030), 687–696.
Bousman, C.A., Dunlop, B.W., 2018. Pharmacogenomics J. 18 (5), 613–622.
Bradshaw, E.M., Kent, S.C., Tripuraneni, V., Orban, T., Ploegh, H.L., Hafler, D.A., Love, J.C., 2008. Clin. Immunol. 129 (1), 10–18.
Cao, J., Sun, T., Grattan, K.T.V., 2014. Sens. Actuators B Chem. 195, 332–351.
Cheow, L.F., Courtois, E.T., Tan, Y., Viswanathan, R., Xing, Q., Tan, R.Z., Tan, D.S.W., Robson, P., Loh, Y.-H., Quake, S.R., Burkholder, W.F., 2016. Nat. Methods 13, 833.
Chokkalingam, V., Tel, J., Wimmers, F., Liu, X., Semenov, S., Thiele, J., Figdor, C.G., Huck, W.T.S., 2013. Lab Chip 13 (24), 4740–4744.
Dhar, M., Lam, J.N., Walser, T., Dubinett, S.M., Rettig, M.B., Di Carlo, D., 2018. Proc. Natl. Acad. Sci. 115 (40), 9986–9991.
Eyer, K., Doineau, R.C.L., Castrillon, C.E., Briseño-Roa, L., Menrath, V., Mottet, G., England, P., Godina, A., Brient-Litzler, E., Nizak, C., Jensen, A., Griffiths, A.D., Bibette, J., Bruhns, P., Baudry, J., 2017. Nat. Biotechnol. 35, 977.
Fiehn, O., 2002. In: Town, C. (Ed.), Functional Genomics. Springer Netherlands, Dordrecht, pp. 155–171.
Freund, A., Jolivel, V., Durand, S., Kersual, N., Chalbos, D., Chavey, C., Vignon, F.,

Lazennec, G., 2004. Oncogene 23, 6105.
He, R., Sang, H., Ye, R.D., 2003. Blood 101 (4), 1572–1581.
Heath, J.R., Ribas, A., Mischel, P.S., 2015. Nat. Rev. Drug Discov. 15, 204.
Hsu, M.N., Wei, S.-C., Guo, S., Phan, D.-T., Zhang, Y., Chen, C.-H., 2018. Small 14 (49), 1802918.
Huebner, A., Srisa-Art, M., Holt, D., Abell, C., Hollfelder, F., deMello, A.J., Edel, J.B., 2007. Chem. Commun. (12), 1218–1220.
Junkin, M., Kaestli, Alicia J., Cheng, Z., Jordi, C., Albayrak, C., Hoffmann, A., Tay, S., 2016. Cell Rep. 15 (2), 411–422.
Konry, T., Dominguez-Villar, M., Baecher-Allan, C., Hafler, D.A., Yarmush, M.L., 2011. Biosens. Bioelectron. 26 (5), 2707–2710.
Lu, Y., Xue, Q., Eisele, M.R., Sulistijo, E.S., Brower, K., Han, L., Amir, E.-a.D., Pe'er, D., Miller-Jensen, K., Fan, R., 2015. Proc. Natl. Acad. Sci. 112 (7), E607–E615.
Lu, Y., Yang, L., Wei, W., Shi, Q., 2017. Lab Chip 17 (7), 1250–1263.
Marcy, Y., Ouverney, C., Bik, E.M., Lösekann, T., Ivanova, N., Martin, H.G., Szeto, E., Platt, D., Hugenholtz, P., Relman, D.A., Quake, S.R., 2007. Proc. Natl. Acad. Sci. U.S.A. 104 (29), 11889–11894.
Martinez-de Dios, J., Ollero, A., 2004. International Conference Image Analysis and Recognition. Springer, pp. 376–383.
Mazutis, L., Gilbert, J., Ung, W.L., Weitz, D.A., Griffiths, A.D., Heyman, J.A., 2013. Nat. Protoc. 8, 870.
Ng, E.X., Sun, G., Wei, S.-C., Miller, M.A., DasGupta, R., Lam, P.Y.P., Chen, C.-H., 2019. Anal. Chem. 91 (2), 1277–1285.
Obenauf, A.C., Zou, Y., Ji, A.L., Vanharanta, S., Shu, W., Shi, H., Kong, X., Bosenberg, M.C., Wiesner, T., Rosen, N., Lo, R.S., Massagué, J., 2015. Nature 520, 368.
Shembekar, N., Hu, H., Eustace, D., Merten, C.A., 2018. Cell Rep. 22 (8), 2206–2215.
Shen, R., Liu, P., Zhang, Y., Yu, Z., Chen, X., Zhou, L., Nie, B., Żaczek, A., Chen, J., Liu, J., 2018. Anal. Chem. 90 (7), 4478–4484.
Spitzer, Matthew H., Nolan, Garry P., 2016. Cell 165 (4), 780–791.
Tadepalli, S., Kuang, Z., Jiang, Q., Liu, K.-K., Fisher, M.A., Morrissey, J.J., Kharasch, E.D., Slocik, J.M., Naik, R.R., Singamaneni, S., 2015. Sci. Rep. 5, 16206.
Tang, L., Casas, J., 2014. Biosens. Bioelectron. 61, 70–75.
Tang, M.Y., Shum, H.C., 2016. Lab Chip 16 (22), 4359–4365.
Teste, B., Descroix, S., 2012. Nanomedicine 7 (6), 917–929.
Tse, H.T.K., Gossett, D.R., Moon, Y.S., Masaeli, M., Sohsman, M., Ying, Y., Mislick, K., Adams, R.P., Rao, J., Di Carlo, D., 2013. Sci. Transl. Med. 5 (212) 212ra163-212ra163.
Wang, B.L., Ghaderi, A., Zhou, H., Agresti, J., Weitz, D.A., Fink, G.R., Stephanopoulos, G., 2014. Nat. Biotechnol. 32 (5), 473–478.
Xue, H., Lu, B., Lai, M., 2008. J. Transl. Med. 6 (1), 52.
Yu, C., Irudayaraj, J., 2007. Anal. Chem. 79 (2), 572–579.